

**Role of exchange and correlation in high-harmonic generation
spectra of H₂, N₂ and CO₂: real-time time-dependent
electronic-structure approaches**

Carlo Federico Pauletti

*Dipartimento di Scienze Chimiche e Farmaceutiche,
via Giorgieri 1, Trieste (Italy) and Sorbonne Universités,
UPMC Univ Paris 06, UMR 7616, Laboratoire de Chimie Théorique,
F-75005 Paris, France. CNRS, UMR 7616,
Laboratoire de Chimie Théorique, F-75005 Paris*

Emanuele Coccia

Dipartimento di Scienze Chimiche e Farmaceutiche, via Giorgieri 1, Trieste (Italy)

Eleonora Luppi

*Sorbonne Universités, UPMC Univ Paris 06,
UMR 7616, Laboratoire de Chimie Théorique,
F-75005 Paris, France. CNRS, UMR 7616,
Laboratoire de Chimie Théorique, F-75005 Paris, France.**

(Dated: October 13, 2020)

Abstract

This study arises from the attempt to answer the following question: how different descriptions of electronic exchange and correlation affect the high-harmonic generation (HHG) spectroscopy of H_2 , N_2 and CO_2 molecules? We compare HHG spectra for H_2 , N_2 and CO_2 with different ab initio electronic structures methods: real-time time-dependent configuration interaction (RT-TD-CIS) and real-time time-dependent density functional theory (RT-TDDFT) using truncated basis sets composed of correlated wave functions expanded on Gaussian basis sets. In the framework of RT-TDDFT, we employ PBE and LC- ω PBE functionals. We study HHG spectroscopy by disentangling the effect of electronic exchange and correlation. We first analyse the electronic exchange alone and in the case of RT-TDDFT with LC- ω PBE, we use $\omega = 0.3$ and $\omega = 0.4$ to tune the percentage of long-range Hartree-Fock exchange and of short-range exchange PBE. Then, we added the correlation as described by PBE functional. All the methods give very similar HHG spectra and they seem not to be particularly sensitive to the different description of exchange and correlation or to the correct asymptotic behaviour of the Coulomb potential. Despite this general trend, some differences are found in the region connecting the cutoff and the background. Here, the harmonics can be resolved with different accuracy depending on the theoretical schemes used. We believe that the investigation of the molecular continuum and its coupling with strong fields merits further theoretical investigations in the next future.

* eleonora.luppi@upmc.fr

I. INTRODUCTION

The optical response of a molecular system in intense ultrashort laser fields is a subject of increasing interest since the advent of attosecond (10^{-18} s) laser pulse generation, characterisation and application. [1–4] In fact, the recent impressive advances in laser technology are continuously triggering the introduction of new time-resolved spectroscopies which offer the opportunity to investigate electron dynamics with unprecedented time resolution. [5–11]

Attosecond pulses may be obtained via the nonlinear optical process high-harmonic generation (HHG) which can be understood semi-classically as a sequence of three steps (three-step model, 3SM): 1) electron ionization in a strong infrared (IR) field, 2) electron acceleration due to the laser field, and 3) electron recombination with the parent ion. During the recombination, coherent XUV and soft X-ray radiation with a sub-femtosecond temporal resolution, i.e. HHG, are emitted. [12, 13]

The electron dynamics implicated in the HHG process can be rather complex [10, 14–17]. Indeed, when the laser interacts with the system a non-stationary electronic wavepacket, consisting of a coherent superposition of excited states, is generated. The time-evolution of the wavepacket involves changing interference and coupling between the different excited states. Moreover, the wavepacket dynamics is determined by parameters of the laser such as intensity, duration, polarisation and phase of carrier frequency.

The proper treatment of the time-dependent electronic wavepacket, and therefore of the many-electron dynamics, under the influence of the laser field is obtained by propagating the time-dependent Schrödinger equation (TDSE). Real-time time-dependent electronic-structure approaches can be conceptually separated in two classes: 1) real-time time-dependent wave function based methods (RT-TDWF), [18–35] and 2) real-time time-dependent density functional theory (RT-TDDFT). [36–46] In RT-TDWF the many-electron dynamics is described by a correlated time-dependent wave function, while in RT-TDDFT the key quantity is the time-dependent density.

Another essential theoretical/computational aspect, common to RT-TDWF and RT-TDDFT, is the strategy used to solve the TDSE. In fact, time propagation can be directly applied to the molecular orbitals (and the amplitudes) [26, 31–33] or to a truncated basis composed of the ground- and excited-state correlated wave functions of the field-free electronic Hamiltonian. [18, 19, 21, 47–49] In the last mentioned approach, for RT-TDDFT,

the excited states are derived in the linear-response Kohn-Sham (KS) framework. [50] In practice, the wave functions are never explicit, but only the TDDFT excitation energies and transition dipole moments are used in the propagation. [18]

In the framework of RT-TDWF, most of the theoretical approaches developed are given by the time-dependent extension of the well-established methods: configuration interaction (CI), coupled cluster (CC) and multiconfigurational self-consistent field (MCSCF). [26, 27, 31, 35, 51–53] Recently, RT-TDWF methods have been applied to investigate HHG in atoms and molecules. The importance of electron correlation in HHG for He, Be, and Ne atoms, was investigated by Sato et al. [27] using real-time time-dependent complete-active-space self-consistent-field (RT-TD-CASSCF) method, and for Ne and Ar atoms by Pathak et al. [53] with time-dependent coupled-electron pair approximation with optimized orbitals (TD-OCEPA0) method. Luppi and Head-Gordon [18] also investigated the role of electron correlation in H_2 and N_2 by using real-time time-dependent configuration interaction with single (RT-TD-CIS) and perturbative-double (RT-TD-CIS(D)) excitations, and real-time time-dependent equation-of-motion coupled-cluster singles and doubles (RT-TD-EOM-CCSD) methods. RT-TD-CIS has been used by some of us to describe the Cooper minimum in the HHG spectrum of Ar atom at different laser intensities [54]. Role of electron correlation in HHG of CO_2 has been investigated by means of the real-time time-dependent propagation of ADC states [24]. The role of HHG as a probe for isomers of polyatomic organic molecules was investigated by Bedurke et al. [29] using RT-TD-CIS and by Wong et al. [28] using a multielectron wave function coupled to Cartesian grid approach.

In the framework of RT-TDDFT, the real interacting many-electron system is usually described by a non-interacting KS system able of reproducing the same density. In the case of a direct propagation, the TDDFT solution of the TDSE for the real system is replaced by the solution of a time-dependent equation which propagates the time-dependent KS orbitals. [55, 56] The many-electron effects are encoded in the time-dependent exchange-correlation potential v_{xc} , which is a functional of the density, and also, in principle, depends on all previous times. However, in most of the cases, the adiabatic approximation is used, i.e. v_{xc} is evaluated at the instantaneous time-dependent density. [57]

To accurately describe the strong-field electron dynamics in RT-TDDFT, it is necessary to correctly reproduce the long-range behaviour of v_{xc} . This permits to reproduce the ionisation threshold energy, giving the onset of the continuum spectrum. Different strategies have been

introduced such as self-interaction corrections (SIC) [58, 59], range-separated functionals [60–63] and long-range corrected potentials. [64, 65]

Instead, the RT-TDDFT approaches that propagate a truncated eigenstate basis, constructed from linear-response TDDFT, describe the many-electron effects through the exchange-correlation kernel f_{xc} . The f_{xc} is the functional derivative of v_{xc} with respect to the density and also needs to be approximated. f_{xc} is nonlocal in time and space, but the most common approximations are adiabatic and only the nonlocality in space is taken into account. In particular, range-separated approaches are among the most successful schemes to model the space dependence. Usually, in these approaches, the exchange part of the f_{xc} , i.e. f_x , is decomposed in a long-range (lr) Hartree-Fock (HF) and a short-range (sr) DFT component: $f_x = f_{x, \text{HF}}^{\text{lr}} + f_x^{\text{sr}}$. The long-range nonlocal exchange kernel permits to better describe Rydberg and ionization potentials, but the lack of frequency-dependence prevents the treatment of doubly excited states. [57]

Recently, RT-TDDFT have been applied to investigate HHG molecules. Monfared et al. [66] studied the effects of inner orbitals in HHG spectra for N_2O , and in particular the role of valence electrons as a way to extend the harmonic plateau by using TDDFT with SIC correction to v_{xc} in the local-density approximation (LDA). The role of inner-valence molecular orbitals was also studied by Chu and Groenenboom et al. [67] for the HHG spectra of N_2 . In this case the LB_α exchange-correlation potential was used for a correct representation of the continuum states. Gorman et al. [68] investigated the structural properties of CO_2 , N_2O and OCS molecules in combination with HHG spectroscopy using TDDFT with SIC corrections to the LDA v_{xc} . Luppi and Head-Gordon [18] also investigated the role of electron correlation in H_2 and N_2 by using RT-TDDFT.

In this work, we have investigated the role of exchange and correlation in HHG spectra of H_2 , N_2 and CO_2 molecules (at fixed internuclear separation) with RT-TD-CIS and RT-TDDFT using a truncated basis composed of the ground- and excited-state correlated wave functions of the field-free electronic Hamiltonian. This basis is represented using Gaussian functions adapted for strong-field processes [69]. At RT-TDDFT level, we have studied the effect of the exchange and correlation on the HHG spectra by means of the PBE [59] and long-range corrected LC- ω PBE functionals, i.e. by means of RT-TD-PBE and RT-TD-LC- ω PBE. [60, 61]. The LC- ω PBE is a range-separated functional which permits to tune the long-range exchange HF and the short-range exchange-correlation DFT functionals.

The article is organised as follows: in Sec. II we introduce the formalism of RT-TD-CIS and RT-TDDFT. The computational method is described in Sec. III and the results are discussed in Sec. IV. Finally in Sec. V, conclusions and perspectives are given. Unless otherwise indicated, atomic units are used throughout this paper.

II. THEORY

The time-dependent Schrödinger equation for a molecular system perturbed by an external time-dependent electric field is given by:

$$i\frac{\partial|\Psi(t)\rangle}{\partial t} = \left(\hat{H}_0 + \hat{V}(t)\right)|\Psi(t)\rangle, \quad (1)$$

where \hat{H}_0 is the time-independent field-free Hamiltonian and $\hat{V}(t) = -\hat{\boldsymbol{\mu}} \cdot \mathbf{E}(t)$ is the time-dependent potential in the length gauge, written in terms of the molecular dipole and the time-dependent electric field $\mathbf{E}(t)$. [18]

We have considered a linearly-polarised electric field $\mathbf{E}(t)$ along the α axis ($\alpha = x, y$ or z), representing a laser pulse,

$$\mathbf{E}(t) = E_0 \mathbf{n}_\alpha \sin(\omega_0 t + \phi) f(t), \quad (2)$$

where E_0 is the maximum field strength, \mathbf{n}_α is a unit vector along the α axis, ω_0 is the carrier frequency, ϕ is the phase, and $f(t)$ is the envelope function chosen as

$$f(t) = \begin{cases} \cos^2(\frac{\pi}{2\sigma}(\sigma - t)) & \text{if } |t - \sigma| \leq \sigma, \\ 0 & \text{else.} \end{cases} \quad (3)$$

where σ is the width of the field envelope.

To solve Eq. (1), the wave function $|\Psi(t)\rangle$ is expanded in a discrete basis of the eigenstates of the field-free Hamiltonian \hat{H}_0 composed of the ground state ($k = 0$) and all the excited states ($k > 0$)

$$|\Psi(t)\rangle = \sum_{k \geq 0} c_k(t) |\Psi_k\rangle, \quad (4)$$

where $c_k(t)$ are time-dependent coefficients. Inserting Eq. (4) into Eq. (1), and projecting

on the eigenstates $\langle \Psi_l |$, gives the evolution equation

$$i \frac{\partial \mathbf{c}(t)}{\partial t} = (\mathbf{H}_0 + \mathbf{V}(t)) \mathbf{c}(t), \quad (5)$$

where $\mathbf{c}(t)$ is the column matrix of the coefficients $c_k(t)$, \mathbf{H}_0 is the diagonal matrix of elements, i.e. $\mathbf{H}_{0,lk} = \langle \Psi_l | \hat{H}_0 | \Psi_k \rangle = E_k \delta_{lk}$ (where E_k is the energy of the eigenstate k), and $\mathbf{V}(t)$ is the non-diagonal matrix of elements, i.e. $\mathbf{V}_{lk}(t) = \langle \Psi_l | \hat{V}(t) | \Psi_k \rangle$. The initial wave function at $t = t_i = 0$ is chosen to be the field-free ground state, i.e. $c_k(t_i) = \delta_{k0}$. To solve Eq. (5), time is discretized and the split-propagator approximation is used which reads as

$$\mathbf{c}(t + \Delta t) \approx e^{-i\mathbf{V}(t)\Delta t} e^{-i\mathbf{H}_0\Delta t} \mathbf{c}(t), \quad (6)$$

where Δt is the time step of the propagation. Since the matrix \mathbf{H}_0 is diagonal, $e^{-i\mathbf{H}_0\Delta t}$ is also a diagonal matrix of elements $e^{-iE_k\Delta t} \delta_{lk}$. The exponential of the non-diagonal matrix $\mathbf{V}(t)$ is calculated as

$$e^{-i\mathbf{V}(t)\Delta t} = \mathbf{U}^\dagger e^{-i\mathbf{V}_d(t)\Delta t} \mathbf{U}, \quad (7)$$

where \mathbf{U} is the unitary matrix describing the change of basis between the original eigenstates of \hat{H}_0 and a basis in which $\hat{V}(t)$ is diagonal, i.e. $\mathbf{V}_d(t) = \mathbf{U}\mathbf{V}(t)\mathbf{U}^\dagger$. [18, 21]

Once the time-dependent wavefunction $|\Psi(t)\rangle$ is known, the time-dependent dipole $\boldsymbol{\mu}(t)$ is computed as

$$\boldsymbol{\mu}(t) = \sum_{lk} c_l^*(t) c_k(t) \langle \Psi_l | \hat{\boldsymbol{\mu}} | \Psi_k \rangle \quad (8)$$

from which, by taking the Fourier transform, the HHG spectrum is obtained

$$P(\omega) = \left| \sum_{lk} \langle \Psi_l | \hat{\boldsymbol{\mu}} | \Psi_k \rangle \frac{1}{t_f - t_i} \int_{t_i}^{t_f} c_l^*(t) c_k(t) e^{-i\omega t} dt \right|^2, \quad (9)$$

where t_i and t_f are the initial and final propagation times.

In the present work we considered in Eq. (4), as truncated basis set, the molecular excited states described at CIS and TDDFT level of theory. The extension of this approach to the solution of the TDSE in the presence of a strong field, brings to the the RT-TD-CIS and RT-TDDFT methods that will be described the next sections.

A. RT-TD-CIS

RT-TD-CIS is the time-dependent extension of the CIS method. [51] In RT-TD-CIS the time-dependent wave function is written on the truncated eigenstate basis of the CIS wave functions

$$|\Psi(t)\rangle = \sum_{k=0} c_k(t) |\Psi_k^{\text{CIS}}\rangle. \quad (10)$$

$|\Psi_k^{\text{CIS}}\rangle$ are constructed by applying the excitation operator $\hat{R} = r_0 + \sum_{ia} r_i^a \hat{a}_a^\dagger \hat{a}_i$ on the Hartree-Fock (HF) description of the field-free system, i.e. $|\Psi_k^{\text{CIS}}\rangle = \hat{R}_k |\phi_0^{\text{HF}}\rangle$. The operator \hat{a}_p^\dagger and \hat{a}_p create and annihilate an electron in the orbital $|\phi_p\rangle$ and the amplitudes r_0 and r_i^a are determined by solving the secular equation $\mathbf{A}\mathbf{X} = \omega^{\text{CIS}}\mathbf{X}$, where $\omega^{\text{CIS}} = E^{\text{CIS}} - E_0^{\text{HF}}$ is the diagonal matrix of the excitation energies, and \mathbf{X} is the matrix of the CIS amplitudes (r_0, r_i^a). E_0^{HF} is the HF ground-state energy. The amplitude r_i^a refers to the Slater determinant associated to the promotion of a single orbital from the occupied orbital i to the virtual a , while r_0 is the CIS amplitude of the HF configuration. The matrix elements of \mathbf{A} are given by

$$A_{ia,jb} = (\epsilon_a^{\text{HF}} - \epsilon_i^{\text{HF}}) \delta_{ij} \delta_{ab} + \langle aj | w_{\text{ee}} | ib \rangle - \langle aj | w_{\text{ee}} | bi \rangle, \quad (11)$$

where $w_{\text{ee}}(r) = 1/r$ is the Coulomb electron-electron interaction (with r the distance between two electrons), $\langle aj | w_{\text{ee}} | ib \rangle$ is the two-electron integral associated with the direct Coulomb and $\langle aj | w_{\text{ee}} | bi \rangle$ is the two-electron integral associated with the Coulomb exchange. The energies ϵ_i^{HF} (ϵ_a^{HF}) are the HF occupied-(virtual)-orbital energies and i, j and a, b refer to the occupied and virtual HF orbitals, respectively.

B. RT-TDDFT

The time-dependent wave function can be formally expanded in the field-free linear-response TDDFT states

$$|\Psi(t)\rangle = \sum_{k=0} c_k(t) |\Psi_k^{\text{TDDFT}}\rangle. \quad (12)$$

As for CIS, the $|\Psi_k^{\text{TDDFT}}\rangle$ can be constructed by applying the excitation operator \hat{R} on the KS ground-state Slater determinant of the field-free system, i.e. $|\Psi_k^{\text{TDDFT}}\rangle = \hat{R}_k |\phi_0^{\text{KS}}\rangle$.

Within the Tamm-Dancoff approximation (TDA), the TDDFT amplitudes are deter-

mined by solving $\mathbf{A}\mathbf{X} = \omega^{\text{TDDFT/TDA}}\mathbf{X}$ where in this case $\omega^{\text{TDDFT/TDA}} = E^{\text{TDDFT/TDA}} - E_0^{\text{KS}}$ is the diagonal matrix of the excitation energies. E_0^{KS} is the KS ground-state energy.

In the adiabatic approximation, the matrix elements of \mathbf{A} are given by:

$$A_{ia,jb} = (\epsilon_a^{\text{KS}} - \epsilon_i^{\text{KS}})\delta_{ij}\delta_{ab} + \langle aj|w_{\text{ee}}|ib\rangle + \langle aj|f_{\text{x}}^{\text{DFT}}|ib\rangle + \langle aj|f_{\text{c}}^{\text{DFT}}|ib\rangle, \quad (13)$$

with ϵ_i^{KS} and ϵ_a^{KS} the KS energies of occupied and virtual orbitals, $\langle aj|w_{\text{ee}}|ib\rangle$ is the two-electron integral associated with the direct Coulomb, $\langle aj|f_{\text{x}}^{\text{DFT}}|ib\rangle$ and $\langle aj|f_{\text{c}}^{\text{DFT}}|ib\rangle$ are, respectively, the DFT exchange and correlation integrals which can be calculated in different density functional approximations. In this work, we used for the $f_{\text{xc}}^{\text{DFT}}$ the PBE functional and its extension in real time will be labelled as RT-TD-PBE.

When the range-separation approach is used, the matrix element $A_{ia,jb}$ in Eq. (13) becomes :

$$A_{ia,jb} = (\epsilon_a - \epsilon_i)\delta_{ij}\delta_{ab} + \langle aj|w_{\text{ee}}|ib\rangle + \langle aj|f_{\text{x}}^{\text{lr},\omega,\text{HF}}|ib\rangle + \langle aj|f_{\text{x}}^{\text{sr},\omega,\text{DFT}}|ib\rangle + \langle aj|f_{\text{c}}^{\text{DFT}}|ib\rangle \quad (14)$$

where $\langle aj|f_{\text{x}}^{\text{lr},\omega,\text{HF}}|ib\rangle = -\langle aj|w_{\text{ee}}^{\text{lr},\omega}|bi\rangle$ is the HF long-range Coulomb exchange, and $\langle aj|f_{\text{x}}^{\text{sr},\omega,\text{DFT}}|ib\rangle$ is the short-range DFT Coulomb exchange. In the integrals, we explicitly indicated the dependence on the parameter ω which controls the range-separation of the Coulomb electron-electron interaction. For $\omega = 0$ the scheme reduces to the usual linear-response TDDFT/TDA, as in Eq. (13). For $\omega = \infty$ the scheme reduces to CIS plus DFT correlation. In this work, we used the scheme LC- ω PBE and its extension in real time will be labelled as RT-TD-LC- ω PBE.

III. COMPUTATIONAL METHODS

In RT-TD-CIS and RT-TDDFT (RT-TD-PBE or RT-TD-LC- ω PBE), the time-dependent wavefunction is expanded using a finite number of electronic excited states and transition dipole moments from the corresponding frequency-domain methods: CIS and TDDFT (PBE or LC- ω PBE). In the case of the LC- ω PBE functional, we used the range-separation parameter $\omega = 0.3$ and $\omega = 0.4$, following Refs [49, 60]. Moreover, in order to decouple the effect of exchange and correlation we also calculated CIS plus PBE correlation (CIS+PBEc) by adding the $\langle aj|f_{\text{c}}^{\text{DFT}}|ib\rangle$ term in Eq. (11), PBE only with exchange (PBEx) and LC- ω PBE

only with exchange (LC- ω PBEx), by removing the $\langle aj|f_c^{\text{DFT}}|ib\rangle$ term from Eq. (13) and Eq. (14).

These frequency-domain methods propagated in time are labelled as : RT-TD-CIS+PBEx, RT-TD-PBEx, and RT-TD-LC- ω PBEx (with $\omega=0.3$ or 0.4). The TDDFT calculations were done within TDA. The dipole matrix elements were taken from field-free calculations by means of the Q-Chem software package [70], and employed in an homemade code, Light [18, 20, 21, 47, 71], that propagates the wavepacket under the influence of a time-dependent strong field.

For all the theoretical methods employed, we used the computational strategy we developed in the recent years which demonstrated to be successful to describe HHG for atomic [21, 54, 72] and small molecular species. [19, 47] We combined Gaussian continuum functions (K) and a heuristic lifetime model with two parameters (d_0 and d_1) for modeling ionization. [19, 21, 54, 72] We used the following Gaussian basis sets with K functions: 6aug-cc-pVTZ+6K for H_2 , 6aug-cc-pVTZ+3K for N_2 and 6aug-cc-pVDZ+6K for CO_2 .

All results correspond to electronic dynamics at fixed nuclear geometries. To enable uniform comparison of the electron dynamics, we performed all calculations at the experimental equilibrium distance of $1.400 a_0$ for H_2 , $2.074 a_0$ for N_2 and $2.209 a_0$ for CO_2 .

We computed HHG spectra for a \cos^2 -shaped laser field (see Eq. (3)) with carrier frequency $\omega_0=0.057 \text{ Ha}$ (1.55 eV , 800 nm), intensity $I=10^{14} \text{ W/cm}^2$ ($d_0=16.478 a_0$ and $d_1=1.414 a_0$). In parenthesis, we reported the values of the escape length parameters used for the heuristic lifetime model.[73] The value of d_0 was chosen on the basis of the three step model, as the maximum electron excursion[54], while d_1 was chosen to remove high-lying above-threshold states. The laser was linearly polarised both perpendicular and parallel to the molecular axis. The duration of the pulse was 20 optical cycles (oc) ($\sigma = 20 \text{ oc}$), where $1 \text{ oc} = 2\pi/\omega_0$. The time step was 0.24 as (0.01 au).

In Tab. (I) we reported the molecular cutoff calculated as $1.32I_p + 3.17U_p$, where I_p is the ionization potential energy and U_p is the ponderomotive energy. [12, 13]. The cutoff energy gives an indication of the maximum photon energy in the harmonic spectrum and it is one of the most important features of any HHG spectrum. In fact, the spectrum is composed of three parts: a perturbative region, where the intensity of the harmonics produced decreases rapidly, a 'plateau' region where the intensity of the harmonics is almost constant and a cutoff region, where the intensity of the harmonics start to decrease until the signal goes

	H ₂	N ₂	CO ₂
RT-TD-CIS	25.92	30.20	30.76
RT-TD-CIS+PBE _c	31.11	31.11	31.73
RT-TD-LC- ω PBE _x ($\omega = 0.4$)	24.44	27.22	27.47
RT-TD-LC- ω PBE ($\omega = 0.4$)	25.06	28.07	28.40
RT-TD-LC- ω PBE _x ($\omega = 0.3$)	23.76	26.38	26.64
RT-TD-LC- ω PBE ($\omega = 0.3$)	24.37	27.22	27.54
RT-TD-PBE _x	20.41	22.82	23.07
RT-TD-PBE	18.85	23.65	23.97

TABLE I. Cutoff for HHG spectrum with $I=10^{14}$ W/cm².

out completely. The cutoff indicates that the extent of the HHG spectrum depends on the nature of the spectroscopic target, via I_p , but also on the intensity and wavelength of the laser, via U_p . In Tab. (II) we also reported the I_p values at different levels of theory, together with the corresponding experimental ones. In the case of H₂ the I_p is minus the HOMO energy, for N₂ is minus the HOMO-2 energy and for CO₂ is the HOMO-3 energy. The choice of the I_p for N₂ and CO₂ was motivated by the inclusion of all possible ionisation channels that have been demonstrated participating to the electron dynamics generating the HHG spectrum. HHG spectra of H₂, N₂ and CO₂ with the perpendicular pulse polarisation are reported in the Supporting Material.

	H ₂	N ₂	CO ₂
I_p^{CIS}	0.594 (76/126)	0.779 (543/458)	0.803 (788/712)
$I_p^{\text{CIS+PBEc}}$	0.623 (78/124)	0.818 (543/460)	0.845 (797/704)
$I_p^{\text{LC-}\omega\text{PBE}_x}_{\omega=0.4}$	0.530 (76/126)	0.650 (512/489)	0.661 (797/704)
$I_p^{\text{LC-}\omega\text{PBE}}_{\omega=0.4}$	0.557 (76/126)	0.687 (513/488)	0.701 (748/752)
$I_p^{\text{LC-}\omega\text{PBE}_x}_{\omega=0.3}$	0.501 (76/126)	0.614 (507/494)	0.625 (740/761)
$I_p^{\text{LC-}\omega\text{PBE}}_{\omega=0.3}$	0.527 (76/126)	0.650 (507/494)	0.664 (742/758)
$I_p^{\text{PBE}_x}$	0.356 (9/193)	0.460 (330/671)	0.471 (529/972)
I_p^{PBE}	0.381 (0/202)	0.496 (329/672)	0.510 (543/957)
I_p^{Exp}	0.567 [74]	0.673[75]	0.711[76]

TABLE II. Ionisation potential energy (I_p) in Hartree for the different theoretical schemes. Experimental values are also reported. In parenthesis we also reported the number of bound states, i.e. below the I_p , and of the number of continuum states, i.e. above the I_p used in the time-dependent propagation..

IV. RESULTS AND DISCUSSION

In the following we will attempt to answer the following question: how different theoretical descriptions of the electronic exchange and correlation can affect the shape of the HHG spectra of the H_2 , N_2 and CO_2 molecular systems?

A. H_2

To understand the role of exchange and correlation in HHG for the H_2 molecule, we started to analyse the truncated basis composed of the ground- and excited-state correlated wave functions from the field-free Hamiltonian, which then define the time-dependent wavepacket in the RT-TD-CIS and in RT-TDDFT frameworks. In Fig. (1) we compared the bound and the continuum energy states of the truncated basis calculated by CIS, LC- ω PBEx ($\omega=0.4$ and $\omega=0.3$) and PBEx. This comparison takes into account only the exchange contribution.

CIS is considered the method of reference as it contains HF exchange with correct asymptotic behaviour of the Coulomb potential ($-1/r$). The comparison with the other methods was done by taking the HF ground state energy as the zero energy reference. In Fig. (1) for each theoretical methods, we also plotted the I_p (see Tab. (II)). In Tab. (II) we also reported the number of bound and continuum states for each theoretical scheme.

Considering the top panel of Fig. (1), we observe that the CIS methods satisfactorily represents the Rydberg states, because of the correct asymptotic behaviour of the Coulomb potential. The I_p in CIS (Tab. (II)) has also the best agreement with the experimental value compared to the other theoretical schemes. Considering PBEx, for which the Coulomb potential decays exponentially at large distances, we observe that it does not support the Rydberg series of bound states. In this case, the I_p has the worst agreement with the experimental value when compared to the other theoretical calculations. This behaviour is also supported by comparing the number of bound states of PBEx in Tab. (II) with the other theoretical methods: the number of computed PBEx bound states is considerably lower. This is consistent with the wrong asymptotic behaviour of the Coulomb exchange potential of PBEx.

The LC- ω PBEx contains a percentage of the HF long-range exchange and of the short-range PBE exchange. In the limit of $\omega = \infty$ the LC- ω PBEx scheme reduces to CIS, while

for $\omega = 0$ the LC- ω PBEx scheme reduces to the PBEx. Therefore, by construction, the LC- ω PBEx with $\omega=0.4$ and $\omega=0.3$ connects the CIS and the PBEx schemes. Considering $\omega=0.4$ the excitation energies are closer to the CIS while for $\omega=0.3$ the excitation energies are closer to the PBEx. The corresponding I_p values in Tab. (II) reflect the same behaviour.

In the bottom panel of Fig. (1), the continuum energy states are compared. The trend is similar to the one observed for the bound states (top panel). However, despite the energy shift between the different methods, the continuum energy density is the same for all the theoretical schemes.

The bound and continuum energy states represented in Fig. (1) are also the energy space in which the electrons move during the propagation, which can affect the description of the HHG spectrum. In Fig. (2) we show how these different electronic-structure descriptions impact the HHG spectrum of H_2 . For each level of theory we also plotted the molecular energy cutoff [12, 13, 19] reported in Tab. (I).

RT-TD-CIS, with the 6aug-ccpVTZ+6K basis set, reproduces well the main features of a HHG spectrum: perturbative/plateau, cutoff and background regions.[19, 47] It is interesting to compare this spectrum with other RT-TD-CIS calculations which used different basis sets. Luppi and Head-Gordon [18] calculated the HHG spectrum for H_2 using various Gaussian basis sets, the largest one being d-aug-cc-pVTZ. The general trend of the HHG spectrum with this basis set is correct. However, for the region just beyond the cutoff, the comparison with the 6aug-cc-pVTZ+6K basis set shows some differences, due to the lack of diffuse functions and optimised K functions for the continuum states.

The HHG spectrum in RT-TD-CIS of the H_2 molecule was also calculated by White et al.[47] using the 6aug-cc-pVTZ and the 6aug-cc-pVTZ with additional basis function centers (ghost atoms). The 6aug-cc-pVTZ and 6aug-cc-pVTZ+6K give the same spectrum up to the 25th harmonic. Next, the lack of optimised Gaussian functions for continuum, makes appear in the 6aug-cc-pVTZ a number of extra (artificial) harmonics which are due to diffuseness of the basis set. For this reason White et al.[47] found a second plateau which is much more pronounced than what we found with the 6aug-cc-pVTZ+6K basis set.

The other approach used by White et al.[47] to correct their basis for the continuum states, was to insert ghost atoms in different geometrical configurations around the H_2 molecule. This technique permits to make disappear some of the spurious harmonics at high energy. Using this strategy makes the second plateau less evident than with 6aug-cc-pVTZ, which

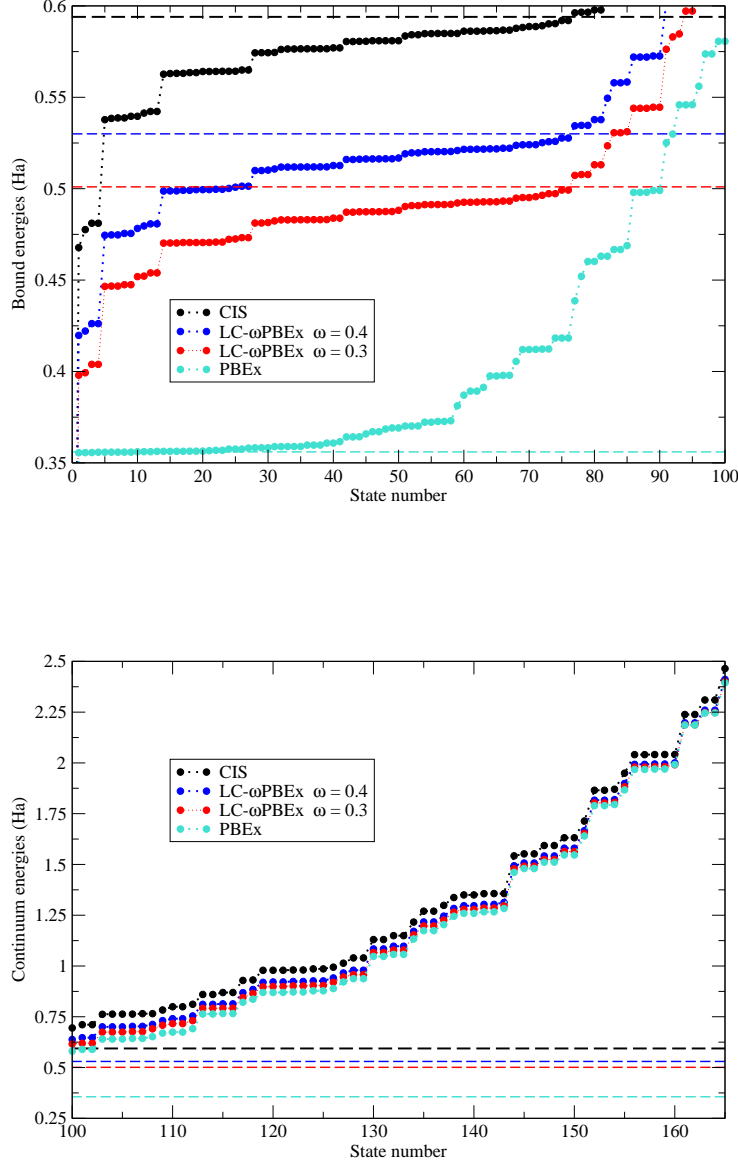


FIG. 1. H₂ excitation energies only with exchange: bound (top, states 0-100) and continuum (bottom, states 100-170) energies for CIS, LC- ω PBEEx with $\omega=0.3$ and $\omega=0.4$ and PBEEx. The I_p is also reported. The panels are a zoom of the energy region of interest for the calculated HHG spectra.

is more in agreement with what we found with 6aug-cc-pVTZ+6K basis set. Comparison between the effects from ghost atoms and K functions is also reported for the HHG spectrum of the hydrogen atom in Ref. [20].

The differences between our HHG spectrum and the one calculated by White et al.[47]

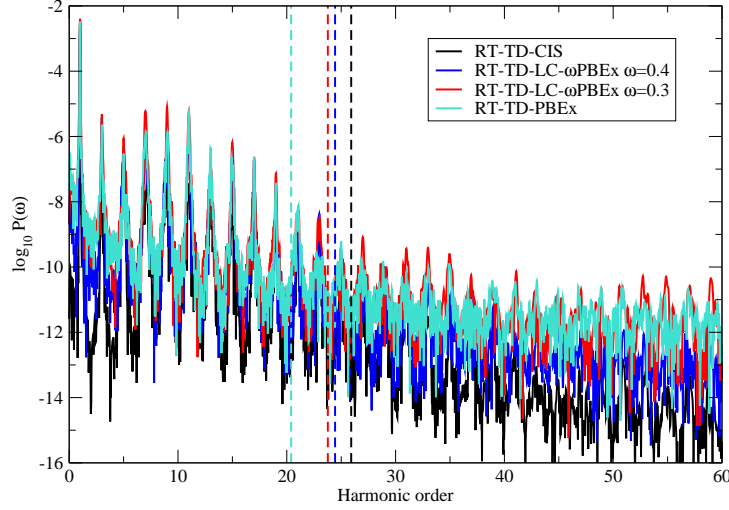


FIG. 2. H_2 : HHG spectra only with exchange for RT-TD-CIS, RT-TD-LC- ω PBEx with $\omega=0.3$ and $\omega=0.4$ and RT-TD-PBEx. The laser has $I=10^{14}$ W/cm 2 , $\omega = 0.057$ Ha and polarisation parallel to the molecular axis.

with ghost atoms can also be due to the different approach to treat ionisation during the propagations. White et al.[47] used a heuristic lifetime model with only one escape length, at variance with what was done by us in this work (Section III). This means that the two HHG spectra differently exclude some recombination processes which proceed through continuum states, including some classes of long-lived resonances.

In Fig. (2) we also report the HHG spectra computed by means of other theoretical approaches. The RT-TD-LC- ω PBEx with $\omega=0.4$ is the closest approach to RT-TD-CIS considering the description of the exchange. In fact, it contains a large percentage of HF exchange and a small percentage of PBE exchange. The effect is an overall increase of the spectrum intensity. The second plateau almost disappears. The RT-TD-LC- ω PBEx with $\omega=0.3$ has a higher percentage of the PBEx with respect to $\omega=0.4$. Also in this case the spectrum intensity is generally increased with respect to RT-TD-CIS. However, some harmonics reappear at higher energy. Considering the HHG in PBEx we observe that the peak intensities in the plateau region are not forcefully higher than with RT-TD-LC- ω PBEx with $\omega=0.3$ but the peaks are certainly more noisy. The most important feature with PBEx is that no second plateau is described. Some harmonics are very badly reproduced or not

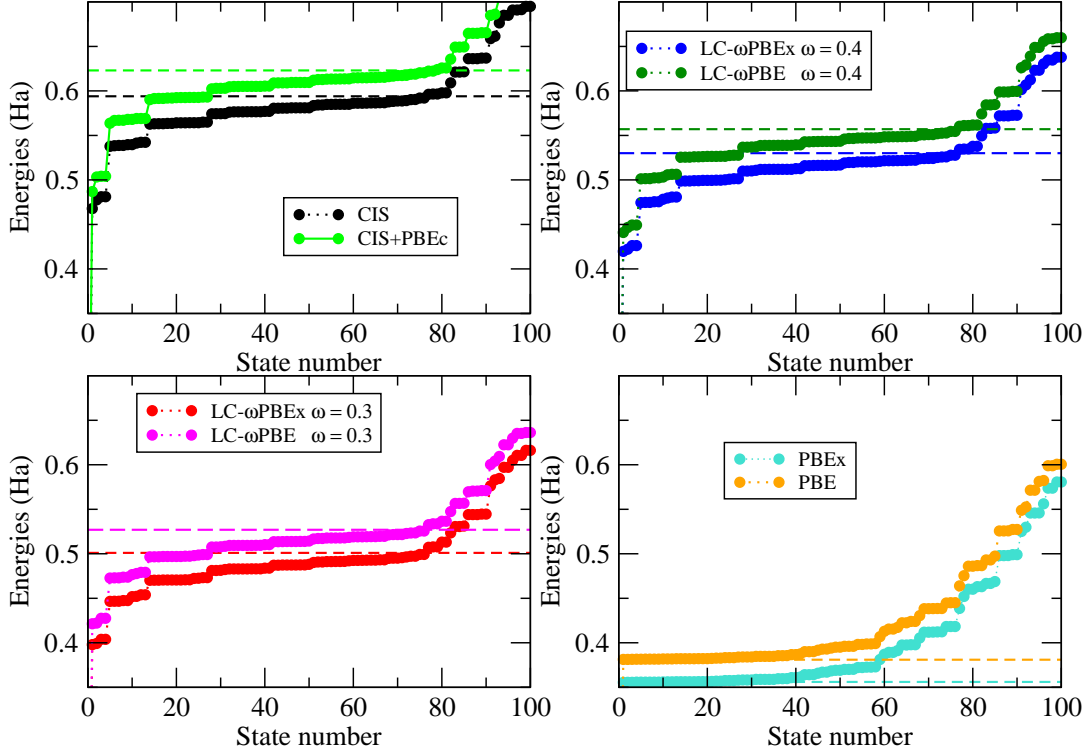


FIG. 3. H_2 excitation energies with exchange and correlation: bound and onset of continuum energies for CIS versus CIS+PBEc, LC- ω PBEx versus LC- ω PBE with $\omega=0.3$ and $\omega=0.4$ and PBEx versus PBE. The I_p is also reported.

even resolved.

To go further with our analysis we include the role of the PBE correlation (PBEc). In Fig. (3) we show the bound and the onset of the continuum energy states calculated by CIS+PBEc, LC- ω PBE ($\omega=0.3$ and $\omega=0.4$) and PBE. The effect is the same for all the theoretical schemes. We obtain a rigid shift of the excitation energies and also of the I_p (see Tab. (II)). It is interesting to note that for the PBE we found no bound states.

In Fig. (4) we analysed the HHG for H_2 by comparing the theoretical schemes with only exchange to the same schemes where we also included the PBEc. In the case of CIS, adding PBEc has very little impact. PBEc slightly lower the intensity of some harmonics. Instead, PBEc has larger impact on LC- ω PBEx ($\omega=0.3$ and $\omega=0.4$) and PBEx. The harmonics in

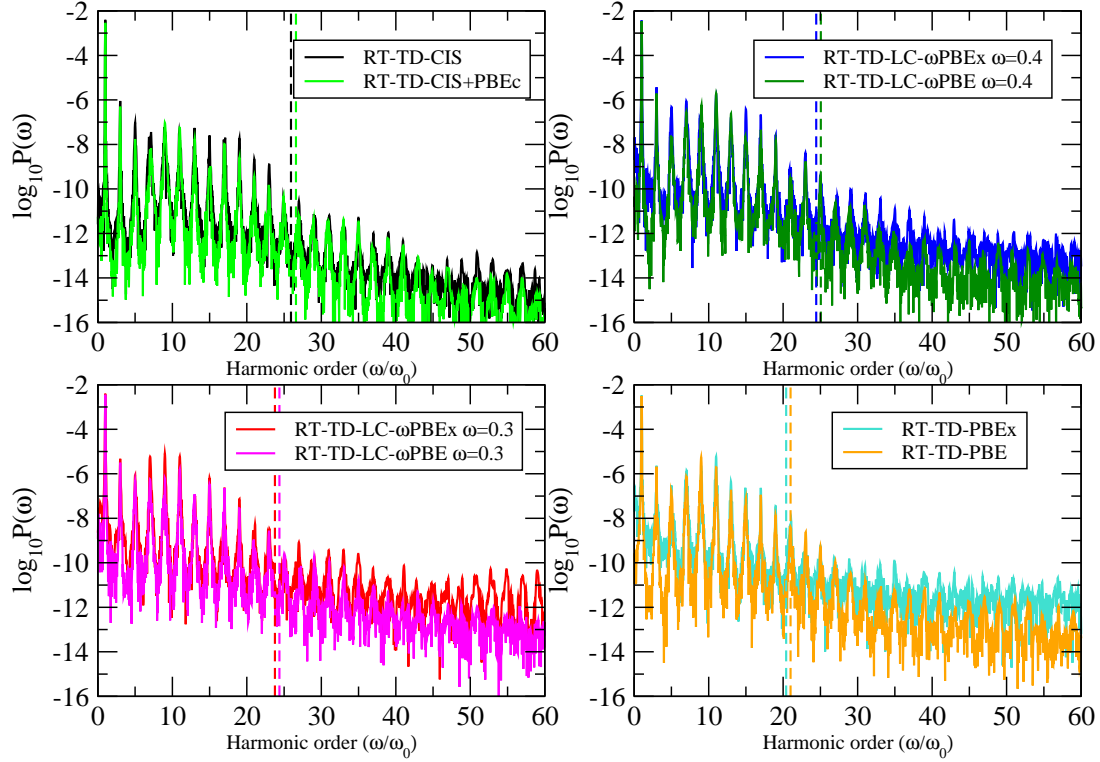


FIG. 4. H_2 : HHG spectra for RT-TD-CIS versus RT-TD-CIS+PBEC, RT-TD-LC- ω PBEx versus RT-TD-LC- ω PBE with $\omega=0.3$ and $\omega=0.4$ and RT-TD-PBEx versus RT-TD-PBE. The laser has $I=10^{14}$ W/cm 2 , $\omega = 0.057$ Ha and polarisation parallel to the molecular axis.

the plateau lower their intensities, but the strongest effect is shown for those harmonics in the region after the cutoff. PBEC seems to lower the background and therefore to better resolve high energy harmonics. Moreover, RT-TD-LC- ω PBE and RT-TDPBE are closer to RT-TD-CIS when PBEC is included.

B. N_2

To understand the role of exchange and correlation in HHG for the N_2 molecule, we compared in Fig. (5) the bound and the continuum energy states calculated by CIS, LC- ω PBEx ($\omega=0.4$ and $\omega=0.3$) and PBEx. These are the energies of the truncated basis used in the RT-TD-CIS and in RT-TDDFT calculations. In Fig. (5) we also plotted the I_p (see

Tab. (II)) for the different levels of theory. We remind that in this case I_p is calculated as minus the HOMO-2 energy. As in the case of the H_2 molecule, the CIS method is our reference because of the correct asymptotic behaviour of the electron Coulomb potential.

In the top panel of Fig. (5) the CIS shows a large number of bound states below the I_p . The behaviour of the other theoretical approaches follows the same trend observed for the H_2 molecule. The plateau structures below I_p indicate the presence of other ionisation channels, related to electron ionisation from HOMO and HOMO-1. In the bottom panel of Fig. (5) the continuum energy states are compared. The trend is similar to the one observed for the bound states (top panel), but less regular than the trend for the continuum of the H_2 molecule.

In Fig. (6) we show the HHG spectra for the different theoretical schemes only including the electron exchange. The general trend already observed in H_2 is reproduced also for N_2 . HHG peaks by RT-TD-PBEx are slightly more intense higher and also more noisy than those described by RT-TD-CIS. The RT-TD-LC- ω PBEx with $\omega=0.3$ behave close to RT-TD-PBEx while RT-TD-LC- ω PBEx with $\omega=0.4$ is similar to RT-TD-CIS.

Luppi and Head-Gordon [18] calculated the HHG spectrum of N_2 in RT-TD-CIS with different Gaussian basis sets. The largest one was the d-aug-cc-pVTZ. From the comparison with our results, obtained with the 6aug-cc-pVTZ+3K basis set, we observe a similar behaviour of the two chosen computational protocols. However, we confirm that as for the H_2 molecule, the critical point is the description of the energy region around the cutoff. The cutoff region is poorly described by the d-aug-cc-pVTZ basis sets, which lacks of a (large) number of diffuse functions and optimised K functions for the continuum states.

To go further in our analysis we include the role of the PBE correlation (PBEC). In Fig. (7) we show the bound and the onset of the continuum energy states calculated by CIS+PBEC, LC- ω PBE ($\omega=0.3$ and $\omega=0.4$) and PBE. The effect is the same for all the theoretical schemes. We obtain a rigid shift of the excitation energies and of the I_p (see Tab. (II)).

In Fig. (8) we analysed the HHG for N_2 by comparing the theoretical schemes with only exchange to the same schemes where we also included the PBEC term. In the case of RT-TD-CIS, adding PBEC has very little impact. PBEC slightly lowers the intensity of some harmonics. Instead, PBEC has larger impact on RT-TD-LC- ω PBEx ($\omega=0.3$ and $\omega=0.4$) and RT-TD-PBEx. The harmonics in the plateau lower their intensities, but the strongest

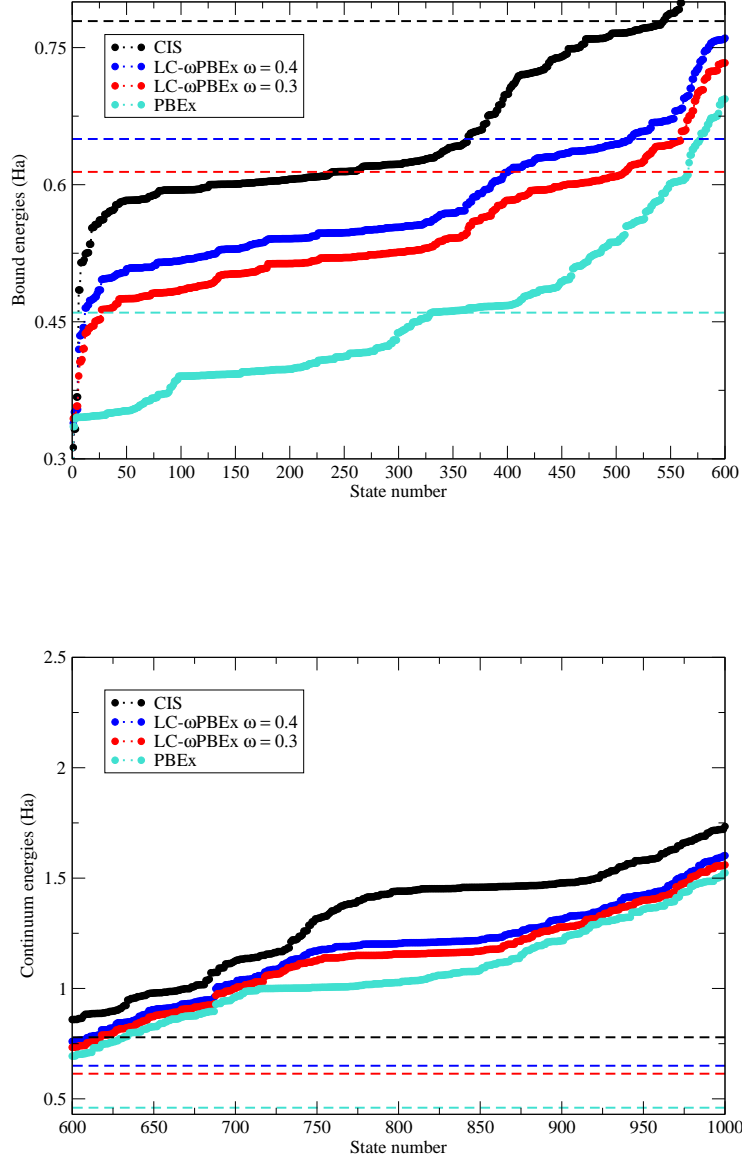


FIG. 5. N₂ excitation energies only with exchange: bound (top, states 0-600) and continuum (bottom, states 600-1000) energies for CIS, LC- ω PBEEx with $\omega=0.3$ and $\omega=0.4$, PBEEx. The I_p is also reported. The panels are a zoom of the energy region of interest for the calculated HHG spectra.

effect is shown for those harmonics in the region after the cutoff. PBEc seems to lower the background and therefore to better resolve high energy harmonics. As for H₂, RT-TD-LC- ω PBE and RT-TD-PBE are characterized by a better agreement with RT-TD-CIS when the PBE correlation is included.

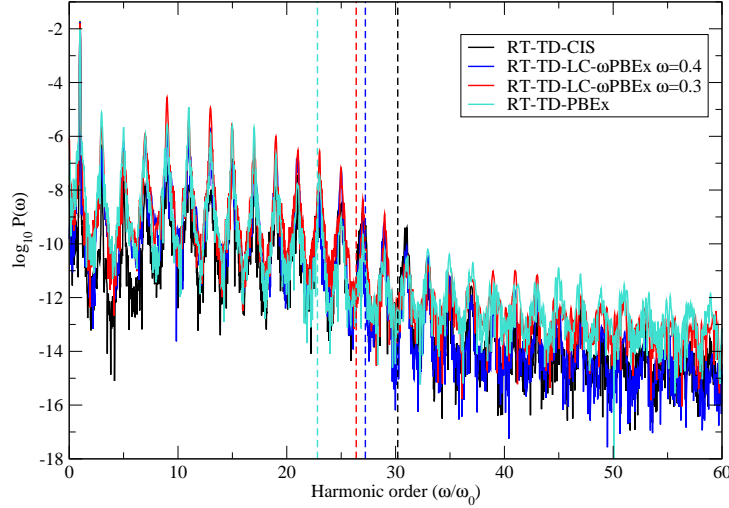


FIG. 6. N_2 : HHG spectra only with exchange for RT-TD-CIS, RT-TD-LC- ω PBEx with $\omega=0.3$ and $\omega=0.4$ and RT-TD-PBEx. The laser has $I=10^{14}$ W/cm 2 , $\omega = 0.057$ Ha and polarisation parallel to the molecular axis.

C. CO_2

In Fig. (9) we show the bound and the continuum energy states calculated by CIS, LC- ω PBEx ($\omega=0.4$ and $\omega=0.3$) and PBEx. These are the energies of the truncated basis used in the RT-TD-CIS and in RT-TDDFT schemes. In Fig. (9) we also plotted the I_p (see Tab. (II)) for the different levels of theory employed here. Again, CIS description of the CO_2 electronic structure can be considered as a theoretical reference, thanks to the correct asymptotic behaviour of the Coulomb potential.

In the top panel of Fig. (9) the behaviour of the bound excitation energies, computed at the various levels of theory, is similar to the trend in H_2 and N_2 . The PBEx largely underestimates the ionization threshold and therefore the continuum energy collapse, whereas increasing the HF character implies a better description of the long-range Coulomb potential and therefore of the bound excitation energies which are then reproduced correctly together with the onset of the continuum. Another important observation is that in the case of CO_2 we observe energy plateau structures which are due to the presence of other ionisation channels, corresponding to the electron removal from HOMO, HOMO-1 and HOMO-2.

In the bottom panel of Fig. (9) the continuum energy states are compared for the different

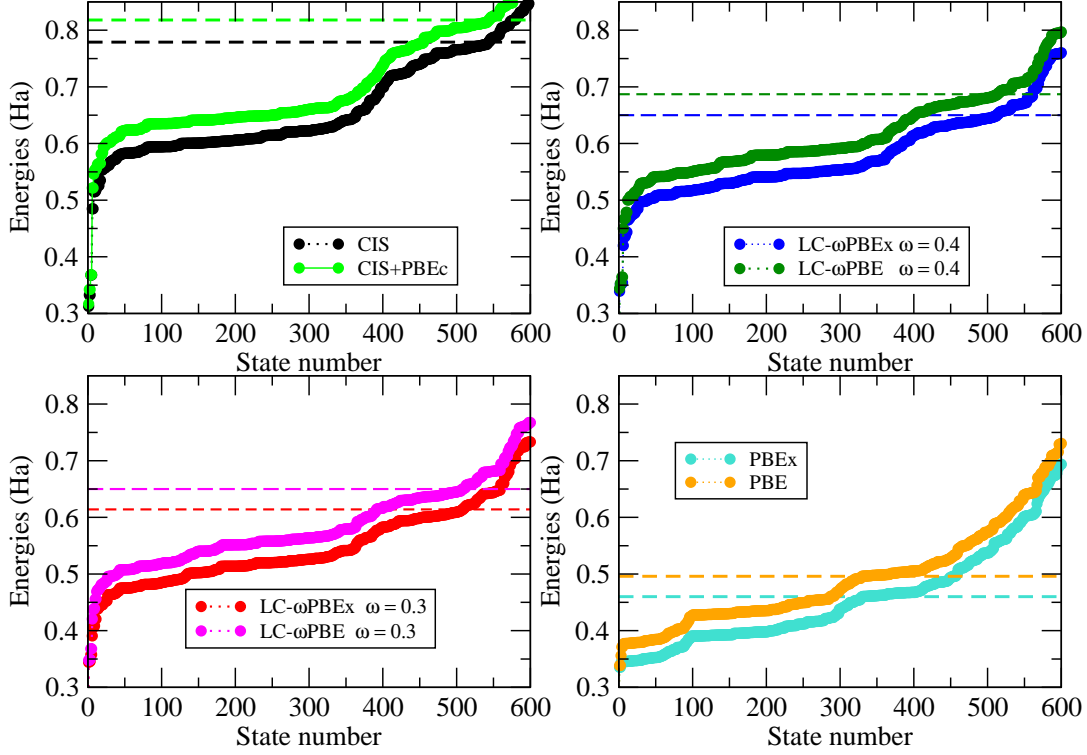


FIG. 7. N_2 excitation energies with exchange and correlation: bound and onset of continuum energies for CIS versus CIS+PBEc, LC- ω PBEx versus LC- ω PBE with $\omega=0.3$ and $\omega=0.4$ and PBEx versus PBE. The I_p is also reported.

theoretical schemes. Also in this case the trend is the same as in H_2 and N_2 , the LC- ω PBEx energies with $\omega=0.3$ and 0.4 lie within the CIS and PBEx ones.

The effect of the different level of theory for electronic exchange and correlation employed to describe the CO_2 wavepacket and therefore the HHG spectra is shown in Fig. (10). RT-TD-CIS and RT-TD-LC- ω PBEx with $\omega=0.3$ and 0.4 have very similar behaviour for plateaux, cutoff and background region. Except for very little differences in the peak intensity concerning the HHG in the plateau region as already observed for H_2 and N_2 . Instead, the behaviour of RT-TD-PBEx is different. The intensity of the HHG spectrum is lower than with the other theoretical methods and in particular for the cutoff and background region. Moreover, it seems that harmonics continue to be present also at high energy, where

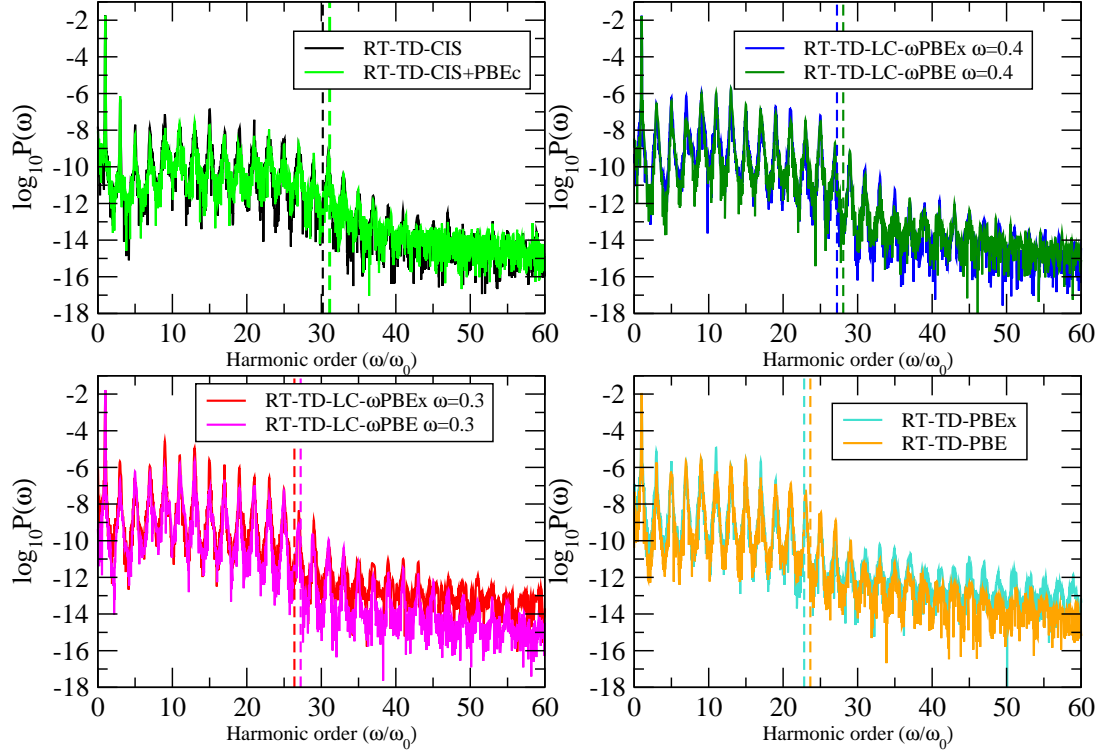


FIG. 8. N_2 : HHG spectra for RT-TD-CIS versus RT-TD-CIS+PBEC, RT-TD-LC- ω PBEx versus RT-TD-LC- ω PBE with $\omega=0.3$ and $\omega=0.4$ and RT-TD-PBEx versus RT-TD-PBE. The laser has $I=10^{14}$ W/cm 2 , $\omega = 0.057$ Ha and polarisation parallel to the molecular axis.

instead the other methods do not describe any HHG anymore.

The effect of PBE correlation on top of the different theoretical schemes with only exchange is shown in Fig. (11) for the excitation energies. The behaviour is consistent with the trend found for H_2 and N_2 .

Including the correlation in the electronic-structure description does not produce any appreciable or systematic change in the HHG spectra, as shown in Fig. (12). The overall effect seems to be smaller than in H_2 and N_2 molecules.

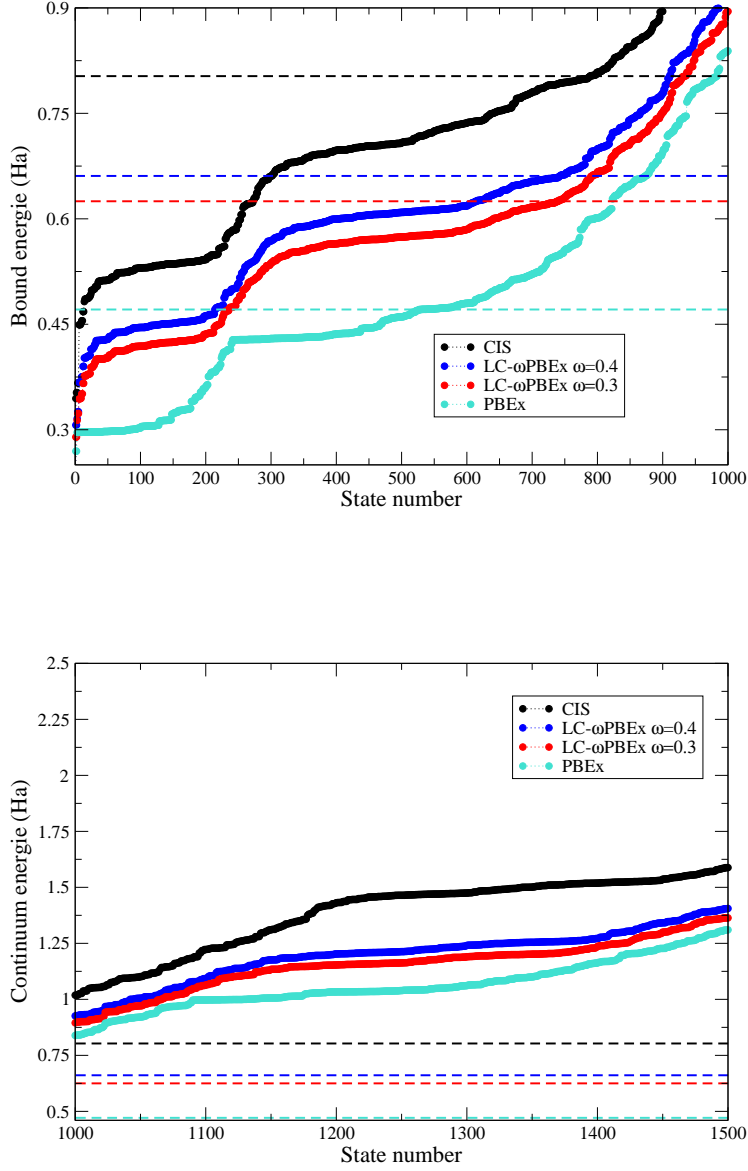


FIG. 9. CO₂ excitation energies only with exchange: bound (top, states 0-1000) and continuum (bottom, states 1000-1500) energies for CIS, LC- ω PBE with $\omega=0.3$ and $\omega=0.4$ and PBE. The I_p is also reported. The panels are a zoom of the energy region of interest for the calculated HHG spectra.

D. Discussion

The physical mechanism at the origin of the HHG nonlinear process is usually described using the 3SM in which an electron is ionized by the laser pulse and subsequently driven

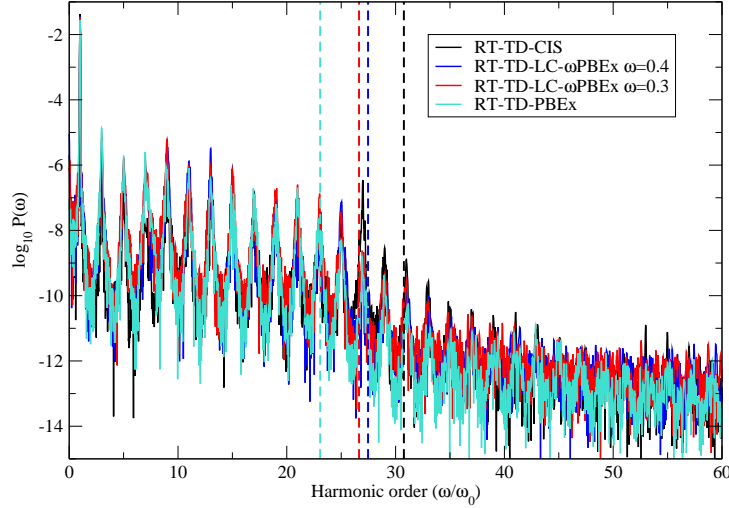


FIG. 10. CO₂ : HHG spectra only with exchange for RT-TD-CIS, RT-TD-LC- ω PBEx with $\omega=0.3$ and $\omega=0.4$ and RT-TD-PBEx. The laser has $I=10^{14}$ W/cm², $\omega = 0.057$ Ha and polarisation parallel to the molecular axis.

far in the continuum by the laser field before finally recombining with the parent ion with the consequent emission of radiation. The 3SM relies on the single active electron (SAE) approximation, which suppose that it is only the outermost electron that contribute to the dynamics while the other electrons are modelled by an effective potential. This implies that the electron correlation is not described and that the 3SM together with the SAE can only be qualitative.

For systems as He where the correlation is small the SAE can be a good approximation [77]. However, for atomic systems such as Be and Ne where the correlation is more important, it was necessary to go beyond the SAE and to use more accurate theoretical approaches [27]. In fact, using correlated methods permitted to describe for Be and Ne a second plateau well extended beyond the first one, and also to identify a resonance peak above the plateau. [78] These features are a clear manifestation of electron correlation. [30]

In molecules the description of the physics beyond the HHG spectroscopy is more complex than in atomic systems. In fact, together with the many-electron dynamics there is also the possibility for the electrons to recombine with multiple atomic centers. An indication of the role of electronic correlation was pointed out by finding a clear correspondance with multiple

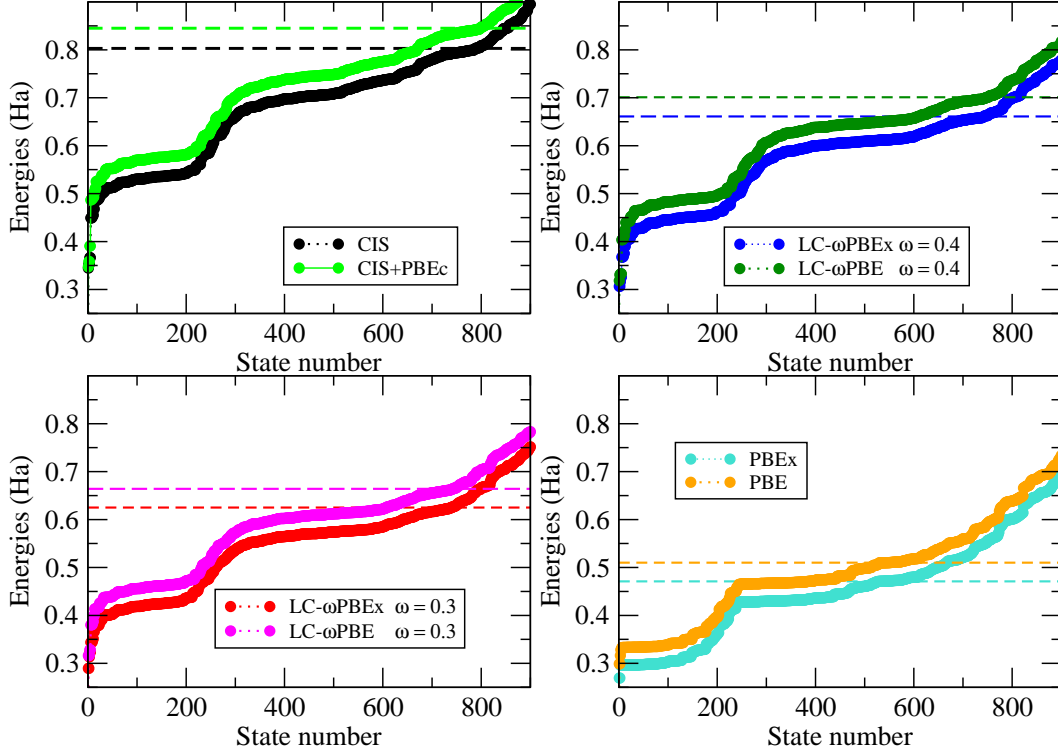


FIG. 11. CO₂ excitation energies with exchange and correlation: bound and onset of continuum energies for CIS versus CIS+PBEC, LC- ω PBEx versus LC- ω PBE with $\omega=0.3$ and $\omega=0.4$ and PBEx versus PBE. The I_p is also reported.

orbital contributions to some specific spectral features of HHG for N₂, O₂, CO₂, F₂, N₂O and CO molecules. [24, 66, 67, 79] Moreover, also for molecules the many-electron dynamics brought evidence of a possible extension of the cutoff. [45]

Understanding how different theoretical schemes can describe the many-electron dynamics under the influence of a strong field, and therefore the HHG spectroscopy, become a fundamental task. We used RT-TD-CIS and RT-TDDFT approaches that propagate a truncated eigenstate basis with different flavours of the electron exchange, on which we added PBE correlation. These approaches demonstrated to reproduce accurate HHG spectra for H₂, N₂ and CO₂, but no large difference among the electronic-structure descriptions was found. This implies that it is important to go beyond the SAE but the HHG is not strongly sensitive

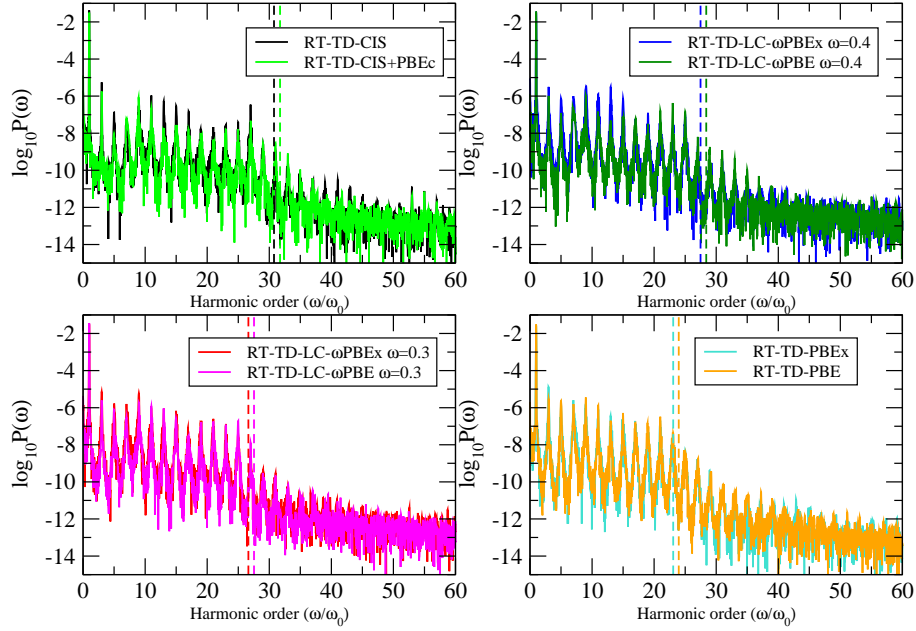


FIG. 12. CO₂ : HHG spectra for RT-TD-CIS versus RT-TD-CIS+PBEc, RT-TD-LC- ω PBEx versus RT-TD-LC- ω PBE with $\omega=0.3$ and $\omega=0.4$ and RT-TD-PBEx versus RT-TD-PBE. The laser has $I=10^{14}$ W/cm², $\omega = 0.057$ Ha and polarisation parallel to the molecular axis.

to the way the electron exchange and correlation is treated. In the context of RT-TDDFT on a numerical grid, Chu and Memoli [45] compared the behaviour of the exchange-correlation potential LB_α and of the local spin-density approximation with self-interaction correction LSDA-SIC to calculate HHG for the H₂ molecule. The exchange-correlation potentials are both corrected for the long-range behaviour of the Coulomb potential. They found that the two methods reproduce very similar HHG which is in agreement with what we have obtained.

A surprising observation by comparing the different methods is that RT-TD-PBE (and RT-TD-PBEx) which wrongly reproduces the asymptotic behaviour of the Coulomb potential, gives HHG spectra rather similar to RT-TD-CIS and RT-TD-LC- ω PBEx ones. Some differences are present in the cutoff and background region but they are very small. This would indicate that the wrong asymptotic behaviour does not play a fundamental role (at least in our computational protocol). However, we want to point out that this result, which

is also related to the self-interaction error, is still rather controversial.

Hsiao-Ling et al. [80] studied the molecular ion H_2^+ . Their work focused on the numerical analysis of the self-interaction error in RT-TDDFT for H_2^+ which has just one electron. Through a comparison with the exact solution of the time-dependent Schrödinger (TDSE) for H_2^+ they showed that LDA and PBE are in agreement with the TDSE for the lowest part of the spectrum but spurious harmonics appear at higher energy. They also studied the performance of the LB94 and of the Fermi-Amaldi scheme plus PBE (LFAsPBE) which have the correct asymptotic behaviour of the Coulomb potential. [80]. They found that LB94 and LFAsPBE are in better agreement with exact TDSE, i.e. the asymptotic behaviour is important. However, they also found that LFAs-PBE is better than LB94 implying that the fine details of the exchange and correlation potential also affect the HHG spectra.

Concerning the HHG of the N_2 molecule, Mack et al. [81] compared LDA and LB94 exchange-correlation potential. Both the approaches can reproduce the main features of the HHG spectra. The LDA has slightly higher intensity but it is still predictive and accurate. Chu and Chu [82] compared the HHG spectra of N_2 using the LSDA without self-interaction correction and LB_α and found 2-3 order of magnitude of difference in the spectra. Therefore they pointed out the importance of incorporating the correct asymptotic long-range potential in the TDDFT treatment of strong field processes. [45]

Wardlow and Dundas [83] studied HHG in benzene comparing LDA incorporating the Perdew-Wang parametrization of the correlation functional with and without self-interaction correction. The agreement between the two methods is very good. They observed an increasing of the plateau harmonics and around the cutoff region, but for the method with the self-interaction correction.

The importance and the role of the long-range Coulomb potential and the electron exchange and correlation merits further theoretical investigations. The methods could have different sensitivity to the laser intensity and to the molecular systems. We believe the most critical point for all these methods is the description of the continuum and how it couples to the electron dynamics during the time-dependent propagation.

V. CONCLUSIONS

In this work we studied the role of electronic exchange and correlation in the HHG spectroscopy of H_2 , N_2 and CO_2 molecules using different ab initio electronic structures methods: RT-TD-CIS and RT-TDDFT (PBE and LC- ω PBE) using truncated basis sets composed of correlated wave functions from the corresponding field-free electronic Hamiltonian.

We computed HHG spectra for a \cos^2 -shaped laser field with carrier frequency $\omega_0=0.057$ Ha (1.55 eV, 800 nm) and intensity $I=10^{14}$ W/cm². We combined Gaussian continuum functions (K) and a heuristic lifetime model with two parameters for modeling ionization. [19, 21, 54, 72]

We separated the effect of exchange from the effect of correlation, by comparing the methods : RT-TD-CIS, RT-TD-LC- ω PBEx ($\omega = 0.3$ and $\omega = 0.4$) and RT-TD-PBEx which contain only electronic exchange. This permitted, without any bias, to observe the effect of the long-range HF and of the short-range PBE on HHG. The correlation was then added in the form of PBE correlation.

All the methods give very similar HHG spectra and they seems not to be particularly sensitive to the different description of exchange and correlation or to the correct asymptotic behaviour of the Coulomb potential. Despite this general trend, some differences are found in the energy region connecting the cutoff and the background. Methods as RT-TD-CIS, RT-TD-LC- ω PBEx ($\omega = 0.4$) and RT-TD-LC- ω PBE ($\omega = 0.4$) which contain long-range HF or at least a percentage of it seems to better resolve the harmonics. However, we believe that the theoretical investigation of the coupling of molecular continuum with strong laser field deserves further investigations.

VI. SUPPLEMENTARY MATERIAL

Data in Supplementary Material refer to the HHG spectra of H_2 , N_2 and CO_2 for the different levels of theory, computed with a pulse polarisation perpendicular to the molecular axis.

VII. DATA AVAILABILITY

Data supporting the findings of this work are available within the article and the supplementary material, and from the corresponding author upon request.

VIII. ACKNOWLEDGEMENTS

C.F.P. acknowledges the Extra Erasmus programme of University of Trieste and Sorbonne Universités for financial support. Authors acknowledge the Computational Center of the University of Trieste.

-
- [1] G. Sansone, Nat. Photonics **14**, 131 (2020).
 - [2] A. J. Uzan et al., Nat. Photonics **14**, 188 (2020).
 - [3] T. Gaumnitz et al., Opt. Express **25**, 27506 (2017).
 - [4] C. Chappuis, D. Bresteau, T. Auguste, O. Gobert, and T. Ruchon, Phys. Rev. A **99**, 033806 (2019).
 - [5] A. Marciniak et al., Nat. Commun. **10**, 337 (2019).
 - [6] P. Peng, C. Marceau, and D. M. Villeneuve, Nat. Rev. Phys. **1**, 144 (2019).
 - [7] M. Ossiander et al., Nature Phys. **13**, 280 (2017).
 - [8] R. Cireasa et al., Nature Phys. **11**, 654 (2015).
 - [9] M. Nisoli, P. Decleva, F. Calegari, A. Palacios, and F. Martín, Chem. Rev. **117**, 10760 (2017).
 - [10] J. Marangos, J. Phys. B **49**, 132001 (2016).
 - [11] A. Dubrouil et al., Nat. Commun. **5**, 4637 (2014).
 - [12] P. B. Corkum, Phys. Rev. Lett. **71**, 1994 (1993).
 - [13] M. Lewenstein, P. Balcou, M. Y. Ivanov, A. L’Huillier, and P. B. Corkum, Phys. Rev. A **49**, 2117 (1994).
 - [14] R. Santra and A. Gordon, Phys. Rev. Lett. **97**, 073906 (2006).
 - [15] A. Gordon, F. Kärtner, N. Rohringer, and R. Santra, Phys. Rev. Lett. **96**, 223902 (2006).
 - [16] S. Beaulieu et al., Phys. Rev. Lett. **117**, 203001 (2016).
 - [17] F. Catoire et al., Phys. Rev. Lett. **121**, 143902 (2018).

- [18] E. Luppi and M. Head-Gordon, *Mol. Phys.* **110**, 909 (2012).
- [19] M. Labeye et al., *J. Chem. Theory Comput.* **14**, 5846 (2018).
- [20] E. Coccia and E. Luppi, *Theor. Chem. Acc.* **135**, 43 (2016).
- [21] E. Coccia et al., *Int. J. Quant. Chem.* **116**, 1120 (2016).
- [22] E. Coccia, R. Assaraf, E. Luppi, and J. Toulouse, *J. Chem. Phys.* **147**, 014106 (2017).
- [23] J. Caillat et al., *Phys. Rev. A* **71**, 012712 (2005).
- [24] M. Ruberti, P. Decleva, and V. Averbukh, *Phys. Chem. Chem. Phys.* **20**, 8311 (2018).
- [25] M. Nest, R. Padmanaban, and P. Saalfrank, *J. Chem. Phys.* **126**, 214106 (2007).
- [26] T. Sato and K. L. Ishikawa, *Phys. Rev. A* **91**, 023417 (2015).
- [27] T. Sato et al., *Phys. Rev. A* **94**, 023405 (2016).
- [28] M. C. H. Wong, J.-P. Brichta, M. Spanner, S. Patchkovskii, and V. R. Bhardwaj, *Phys. Rev. A* **84**, 051403(R) (2011).
- [29] F. Bedurke, T. Klamroth, P. Krause, and P. Saalfrank, *J. Chem. Phys.* **150**, 234114 (2019).
- [30] I. Tikhomirov, T. Sato, and K. L. Ishikawa, *Phys. Rev. Lett.* **118**, 203202 (2017).
- [31] P. Krause, T. Klamroth, and P. Saalfrank, *J. Chem. Phys.* **123**, 074105 (2005).
- [32] C. Huber and T. Klamroth, *Appl. Phys. A* **87**, 93 (2005).
- [33] P. Krause, T. Klamroth, and P. Saalfrank, *J. Chem. Phys.* **127**, 034107 (2007).
- [34] N. Rohringer, A. Gordon, and R. Santra, *Phys. Rev. A* **74**, 043420 (2006).
- [35] T. Sato and K. L. Ishikawa, *Phys. Rev. A* **88**, 023402 (2013).
- [36] N. Tancogne-Dejean et al., *J. Chem. Phys.* **152**, 124119 (2020).
- [37] T. P. Rossi, M. Kuisma, M. J. Puska, R. M. Nieminen, and P. Erhart, *J. Chem. Theory Comput.* **13**, 4779 (2017).
- [38] P. Wopperer, P.M.Dinh, P.-G. Reinhard, and E. Suraud, *Phys. Rep.* **562**, 1 (2015).
- [39] C.-Z. Gao and P. M. Dinh and P.-G. Reinhard and E. Suraud, *Phys. Chem. Chem. Phys.* **19**, 19784 (2017).
- [40] M. Vincendon, L. Lacombe, P. M. Dinh, E. Suraud, and P. G. Reinhard, *Comput. Mater. Sci.* **138**, 426 (2017).
- [41] J. Pilmè, E. Luppi, J. Berés, C. Hoée-Levin, and A. de la Lande, *J. Mol. Mod.* **20**, 2368 (2014).
- [42] X. Wu et al., *J. Chem. Theory Comput.* **13**, 3985 (2017).
- [43] X. Wu, A. Alvarez-Ibarra, D. Salahub, and A. de la Lande, *Eur. J. Phys. D* **72**, 206 (2018).

- [44] A. Parise et al., J. Phys. Chem. Lett. **9**, 844 (2018).
- [45] X. Chu and P. J. Memoli, Chem. Phys. **391**, 83 (2011).
- [46] F. Ding, W. Liang, C. T. Chapman, C. M. Isborn, and X. Li, J. Chem. Phys. **135**, 164101 (2011).
- [47] A. White, C. J. Heide, P. Saalfrank, M. Head-Gordon, and E. Luppi, Mol. Phys. **114**, 947 (2016).
- [48] J. A. Sonk, M. Caricato, and H. B. Schlegel, J. Phys. Chem. A **115**, 4678 (2011).
- [49] J. A. Sonk and H. B. Schlegel, J. Phys. Chem. A **115**, 11832 (2011).
- [50] M. E. Casida, Time-dependent density functional response theory for molecules, in Recent Advances in Density Functional Methods, edited by D. P. Chong, Part I, page 155, World Scientific, Singapore, 1995.
- [51] A. Dreuw and M. Head-Gordon, Chem. Rev. **105**, 4009 (2005).
- [52] T. Sato, H. Pathak, Y. Orimo, and K. L. Ishikawa, J. Chem. Phys. **148**, 051101 (2018).
- [53] H. Pathak, T. Sato, and K. L. Ishikawa, J. Chem. Phys. **152**, 124115 (2020).
- [54] E. Coccia and E. Luppi, Theor. Chem. Acc. **138**, 96 (2019).
- [55] E. Runge and E. K. U. Gross, Phys. Rev. Lett. **52**, 997 (1984).
- [56] E. K. U. Gross and W. Kohn, Phys. Rev. Lett. **55**, 2850 (1985).
- [57] P. Elliott, S. Goldson, C. Canahui, and N. T. Maitra, Chem. Phys. **391**, 110 (2011).
- [58] J. Perdew, Chem. Phys. Lett. **64**, 127 (1979).
- [59] J. Perdew and A. Zunger, Phys. Rev. B **23**, 5048 (1981).
- [60] O. A. Vydrov and G. E. Scuseria, J. Chem. Phys. **125**, 234109 (2006).
- [61] O. A. Vydrov, J. Heyd, A. V. Krukau, , and G. E. Scuseria, J. Chem. Phys. **125**, 074106 (2006).
- [62] J.-D. Chai and M. Head-Gordon, J. Chem. Phys. **131**, 174105 (2009).
- [63] F. Zapata, E. Luppi, and J. Toulouse, J. Chem. Phys. **150**, 234104 (2019).
- [64] R. van Leeuwen and E. Baerends, Phys. Rev. A **49**, 2421 (1994).
- [65] N. Gauriot, V. Vénier, and E. Luppi, J. Chem. Phys. **151**, 234111 (2019).
- [66] M. Monfared, E. Irani, and R. Sadighi-Bonabi, J. Chem. Phys. **148**, 234303 (2018).
- [67] X. Chu and G. C. Groenenboom, Phys. Rev. A **93**, 013422 (2016).
- [68] T. T. Gorman et al., J. Chem. Phys. **150**, 184308 (2019).

- [69] K. Kaufmann, W. Baumeister, and M. Jungen, *J. Phys. B: At. Mol. Opt. Phys.* **22**, 2223 (1989).
- [70] Y. Shao et al., *Phys. Chem. Chem. Phys.* **8**, 3172 (2006).
- [71] E. Luppi and M. Head-Gordon, *J. Chem. Phys.* **139**, 164121 (2013).
- [72] E. Coccia, *Mol. Phys.* (2020), DOI: 10.1080/00268976.2020.1769871.
- [73] S. Klinkusch, P. Saalfrank, and T. Klamroth, *J. Chem. Phys.* **131**, 114304 (2009).
- [74] D. Shiner, J. M. Gilligan, B. M. Cook, and W. Lichten, *Phys. Rev. A* **47**, 4042 (1993).
- [75] A. Hamnett, W. Stoll, and C. E. Brion, **8**, 367 (1976).
- [76] K. Kimura, S. Katsumata, Y. Achiba, T. Yamazaki, and S. Iwata, in Handbook of HeI Photoelectron Spectra.
- [77] R. Reiff, T. Joyce, A. Jaroń-Becker, and A. Becker, *J. Phys. Commun.* **4**, 065011 (2020).
- [78] Y. Li, T. Sato, and K. L. Ishikawa, *Phys. Rev. A* **99**, 043401 (2019).
- [79] J. Heslar, D. Telnov, and S.-I. Chu, *Phys. Rev. A* **83**, 043414 (2011).
- [80] H.-L. Sun, W.-T. Peng, and J.-D. Chai, *RSC Adv.* **6**, 33318 (2016).
- [81] M. R. Mack, D. Whitenack, and A. Wasserman, *Chem. Phys. Lett.* **558**, 15 (2013).
- [82] X. Chu and S.-I. Chu, *Phys. Rev. A* **64**, 063404 (2001).
- [83] A. Wardlow and D. Dundas, *Phys. Rev. A* **93**, 023428 (2016).